

RSRP-Assisted 5G Measurement Time-Based Position Method

Hailong Ren^{1,*}, Wen Liu^{1,*}, Zhongliang Deng¹, Kai Luo¹, Ziyao Ma¹ and Jizhou Wang¹

¹School of Electronics Engineering, Beijing University of Posts and Telecommunications, Beijing 100089, China

Abstract

5G positioning is characterized by high bandwidth and high spectrum utilization, providing faster speeds and larger capacities. As part of human society's infrastructure, it can offer convenience that UWB positioning cannot provide. 5G positioning includes traditional ranging positioning and AI-based fingerprint positioning. However, there are significant impacts on positioning accuracy due to delay errors and clock jitter in current 5G TOA measurements. Fingerprint positioning algorithms based on 5G RSRP demonstrate high precision, but may require retraining of the network after long-term environmental changes. In this paper, we propose a 5G TOA positioning algorithm aided by RSRP information to compensate for Tx-Rx delay errors and mitigate errors caused by clock jitter using a designed clipping and smoothing filter for TOA data. Finally, the two positioning results are weighted and fused based on a residual strategy. When the residual value exceeds a set threshold, only the TOA information with Tx-Rx error compensation is used for positioning, avoiding frequent data collection. Experimental results demonstrate that the algorithm achieves a root mean square error of 0.68m, obtaining satisfactory positioning results.

Keywords

5G positioning, RSRP, time measurement, Tx-Rx delay, clock jitter

1. Introduction

5G, as the representative of the new generation of mobile communication technology, not only provides faster data transmission speeds and more reliable connections but also offers many other important applications, one of which is positioning technology [1]. In the field of 5G positioning, there are currently two main approaches. One approach involves purely AI-based methods for positioning [2], where signal amplitude/phase characteristics or image information are used to construct corresponding fingerprint databases for matching and classifying positioning. The other approach is based on traditional geometric calculations for positioning [3], utilizing device measurements (time/angle) for positioning calculations.

In recent years, machine learning-based positioning methods have achieved sub-meter or even higher positioning accuracy with the development of artificial intelligence technology. However,

Proceedings of the Work-in-Progress Papers at the 13th International Conference on Indoor Positioning and Indoor Navigation (IPIN-WiP 2023), September 25 - 28, 2023, Nuremberg, Germany

*Corresponding author.

✉ sans_bupt@bupt.edu.cn (H. Ren); liuwen@bupt.edu.cn (W. Liu); dengzhl@bupt.edu.cn (Z. Deng); luokai@bupt.edu.cn (K. Luo); mzy123@bupt.edu.cn (Z. Ma); jizhou@bupt.edu.cn (J. Wang)

ORCID 0000-0001-6725-0782 (H. Ren); 0000-0002-6450-1969 (W. Liu)

 © 2023 Copyright for this paper by its authors. Use permitted under Creative Commons License Attribution 4.0 International (CC BY 4.0).

 CEUR Workshop Proceedings (CEUR-WS.org)

when using such methods for long-term positioning, additional human and material resources are required to update fingerprint database data or retrain networks in order to maintain high positioning accuracy as time and environmental conditions change [4]. Traditional positioning methods based on time/angle measurements are more convenient, as they only require solving for the coordinates to be positioned based on geometric relationships after receiving signal measurements. However, due to the nanosecond-level (1 ns can result in a distance error of 0.3m) Tx-Rx delay errors generated during the process from generating digital signals at the baseband to transmitting/receiving RF signals from the antenna [5], as well as the observation value fluctuations caused by clock jitter, significant positioning errors can occur.

In the field of fingerprint positioning, researchers have addressed the issue of updating fingerprint databases by employing additional hardware devices. For instance, [6] proposed using sensors to assist in updating fingerprint database data by simulating signal distribution using ray tracing simulation software with building maps, based on the measured signals from deployed WiFi detectors. [7] introduced a crowd-sourcing approach for updating fingerprint databases, where smartphones' sensors and indoor signal landmarks are utilized for the update process.

In terms of time-based measurements, typically, the Tx-Rx delay is calibrated in advance to minimize the impact of this time delay on positioning accuracy [5]. Filtering techniques are employed to handle the fluctuations in the observed values. However, calibration may not be perfect, and the calibrated time error values can still reach several nanoseconds or even tens of nanoseconds. To address the remaining time delay errors after calibration, 3GPP introduced the concept of a high-confidence reference terminal in Rel-17 to mitigate Tx-Rx delays [8]. Although this approach effectively eliminates such errors, deploying additional reference terminals incurs higher costs. Regarding the removal of observation value jitter, common filtering strategies include arithmetic averaging filtering [9] and first-order inertia filtering [10]. These filtering algorithms demonstrate good jitter removal performance in the presence of slow fluctuation interference but have lower sensitivity and cannot effectively eliminate jitter in rapidly fluctuating data that is still undergoing slow changes.

To compensate for the Tx-Rx delay errors and clock jitter between base stations and positioning devices without relying on additional hardware devices and at a lower cost, while leveraging the advantages of high initial positioning accuracy achieved through AI-based methods, this paper proposes a 5G TOA positioning method assisted by RSRP information. The proposed method utilizes a historical trajectory RNN network to regress and generate virtual ground truth points, which are used to compensate for the Tx-Rx delay error. To address data fluctuations, a designed clamping-smoothing filter is employed to mitigate errors caused by clock jitter and smooth the TOA data. The Ilop-Kalman positioning algorithm is then applied to solve the TOA data, and the Taylor algorithm is utilized to approximate the ground truth points, resulting in a more accurate positioning outcome closely aligned with the actual trajectory.

The remaining sections of this paper are structured as follows. Section 2 presents the design framework and specific details of the algorithms used in this study. It provides an overview of the algorithm's design and explains its key components in detail. Section 3 focuses on the experimental conditions, presenting the corresponding positioning results and conducting an analysis of the outcomes. Finally, in Section 4, a comprehensive summary of the paper is provided, along with an outlook on areas that require further improvement.

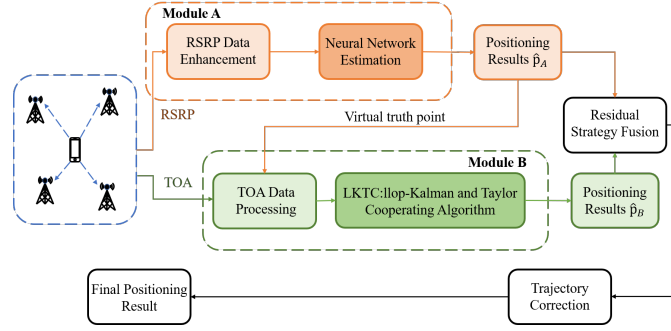


Figure 1: Algorithm framework

2. Positioning Methods

The algorithm framework for 5G TOA positioning assisted by RSRP information is shown in **Figure 1**.

In Module A, firstly, a small amount of RSRP data with real coordinates (x, y) labels is utilized in this paper to train an MLP model that fits the RSRP channel attenuation. Subsequently, based on the well-fitted channel attenuation model, RSRP data with pseudo labels is generated to expand the training set. Then, a recurrent neural network (RNN) with historical trajectory constraints is employed to regress and estimate the positioning coordinates.

In Module B, the raw TOA data is first subjected to data preprocessing. Subsequently, the preprocessed data is processed through the llop-Kalman Taylor Collaborative Algorithm module for solving.

In the positioning fusion and trajectory correction part, we fuse the positioning results from Module A and Module B based on the residual and variance strategy, correct the fusion results based on existing prior information, and obtain the final positioning coordinates.

2.1. Module A: Neural Network-based Location Estimation

The neural network estimation module is shown in **Figure 2**, which mainly includes the data augmentation and historical trajectory RNN network parts.

2.1.1. RSRP Data Enhancement

To improve the generalization ability of the model, we employ neural networks to fit the wireless channel propagation characteristics and systematically generate more training samples. In the process of wireless signal propagation, the signal is transmitted from the transmitter, passes through the wireless channel, and finally arrives at the receiver. The fitting process of the wireless channel propagation model using machine learning methods is data-driven. It involves training the model using existing training data to obtain the model's training parameters. Subsequently, the model is used to predict the signal strength for the data to be predicted, thereby achieving the purpose of expanding the dataset.

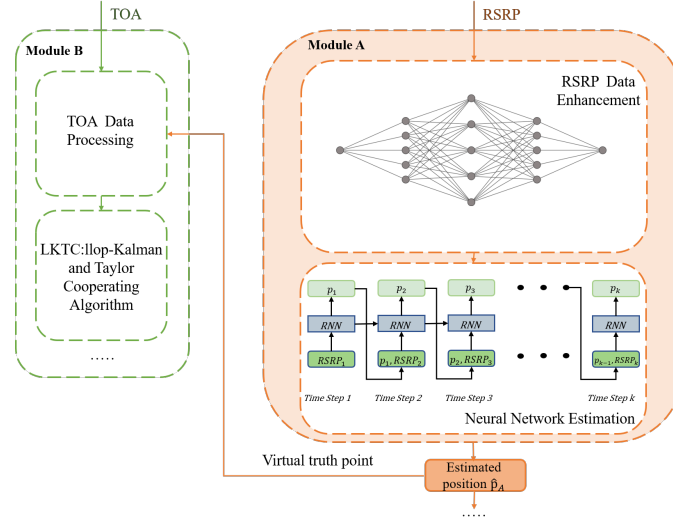


Figure 2: Module A Framework

2.1.2. Historical Trajectory RNN Network

In the subsequent location calculation section, considering that the test data for the competition is the RSRP fingerprint collected by the car moving along a continuous trajectory, using only single-point matching for locating the moving target may result in significant positioning errors. The location of a dynamic target is constrained by space and time. Based on this, we adopted a recursive neural network (RNN) for RSRP fingerprint indoor positioning [11]. Unlike traditional fingerprint positioning, which relies only on fingerprint information at a single point for positioning, the RNN considers the correlation between RSRP measurements in a continuous trajectory, and takes into account the spatial and temporal constraints of the motion trajectory on the basis of single-point matching. This approach establishes the relationship between the time and location information of RSRP in the trajectory, and transforms the discrete positioning task into a continuous time-series feature discovery task.

2.2. Module B: TOA Estimation

The TOA solving process is illustrated in **Figure 3** and mainly consists of TOA data preprocessing and the LKTC module.

2.2.1. TOA Data Processing

Due to the presence of factors such as Tx-Rx delay errors, outliers, and clock jitter in the raw TOA data, preprocessing of the original TOA data is necessary. In the previous section, we obtained the estimated virtual ground truth points in Module A.

$$\hat{P}_{A_k} = (\hat{x}_{vr}, \hat{y}_{vr}) \quad (1)$$

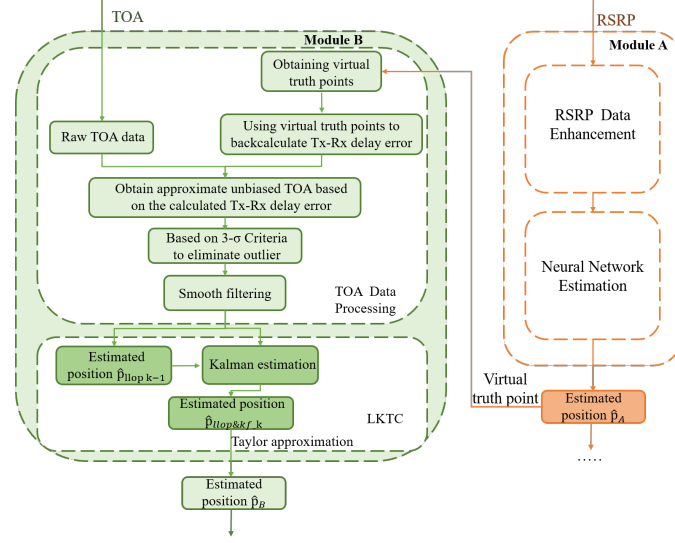


Figure 3: Module B Framework

The observation obtained by base station i has the following relationship with the true position (x, y) of the UE:

$$T\hat{O}A_i = \sqrt{(x_i - x)^2 + (y_i - y)^2} + \delta_{Tx-Rx} \quad (2)$$

where x_i, y_i are the coordinates of base station i , x and y are the true position of the UE, $T\hat{O}A_i$ is the observation measured by the base station, and δ_{Tx-Rx} is the Tx-Rx delay error between the base station and the UE.

This makes it so that

$$(\hat{x}_{vr}, \hat{y}_{vr}) \approx (x, y) \quad (3)$$

Therefore, we can calculate the approximate Tx-Rx delay error of base station i at the k -th sampling point.

$$\delta_{(Tx-Rx)_i}^k = T\hat{O}A_i - \sqrt{(x_i - \hat{x}_{vr})^2 + (y_i - \hat{y}_{vr})^2} - \sum_{e=\min\ error}^{\max\ error} e f(e) \quad (4)$$

When multiple points are measured, the mean of δ_{Tx-Rx} is used as the compensation value for the Tx-Rx delay error in the positioning system. Let e represent the positioning error in Module A, and $f(e)$ represent the probability density function of the error.

$$\hat{\delta}_{(Tx-Rx)_i} = \frac{1}{m} \sum_{n=1}^m \delta_{(Tx-Rx)_i}^n \quad (5)$$

Substitute the result of equation (5) into equation (2), approximately

$$\delta_{Tx-Rx} \approx \hat{\delta}_{(Tx-Rx)_i} \quad (6)$$

By approximately subtracting the Tx-Rx error term from equation (2), the delay error is alleviated

After approximating the Tx-Rx delay error, this paper corrects the outliers in the received data based on the $3\text{-}\sigma$ criterion. At this point, due to clock jitter, the observation of the same location point by the base station fluctuates up and down, and considering that the object is still moving slowly at an irregular speed and direction, based on a naive idea, the designed limited amplitude smoothing filter should correct the case where there is a large difference between two sampling points. The pseudo code for the filter is shown as follows:

Algorithm 1 Limiting smoothing filter

Input: TOA^k, TOA^{k-1}

Output: TOA^k_{smooth}

- 1: $Factor = M$ (M is a constant)
 - 2: $Diff = abs(TOA^k - TOA^{k-1})$
 - 3: **if** ($Diff \geq Factor$) **then**
 - 4: **if** ($TOA^k > TOA^{k-1}$) **then**
 $TOA^k_{smooth} = TOA^{k-1} + Factor$
 - 5: **else**
 $TOA^k_{smooth} = TOA^{k-1} - Factor$
 - 6: **end if**
 - 7: **else**
 $TOA^k_{smooth} = TOA^k$
 - 8: **end if**
-

To determine the appropriate threshold for the Factor value, this paper conducted multiple experiments on the raw data using different down-sampling methods, and obtained the results shown in **Figure 4**.

From Figure 4, it can be observed that as the sampling time interval increases, the minimum RMSE value gradually increases, and the corresponding factor value also increases gradually.

After preprocessing the raw TOA data, the resulting output is shown in **Figure 5**.

Figure 5 displays the plots of TOA samples over time for the four base stations. In the transition from point a to b, the Tx-Rx delay errors are removed. From point b to c, the abrupt changes in b are corrected based on the $3\text{-}\sigma$ principle. After applying the amplitude-limited smoothing filter, the resulting smoothed TOA data is shown in Figure d.

2.2.2. LKTC: Ilop-Kalman Filter Taylor Cooperating Algorithm

In the Ilop part, we can obtain the following relationship between N indoor base stations and the coordinates to be solved :

$$(x_i - x)^2 + (y_i - y)^2 = r_i^2, i = 1, 2, \dots, N \quad (7)$$

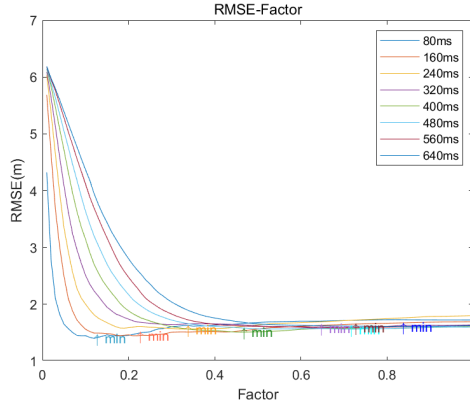


Figure 4: The Factor and corresponding RMSE under different sampling time intervals.

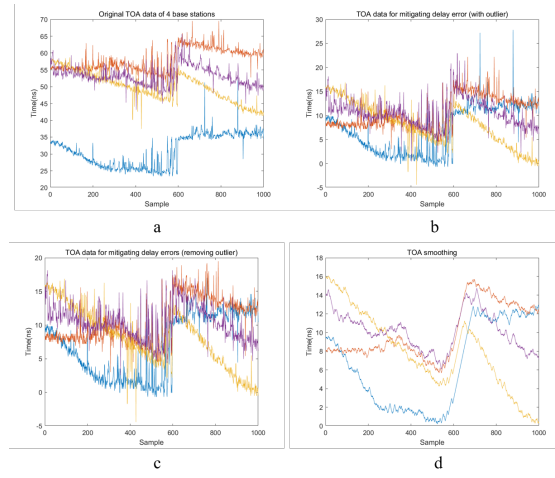


Figure 5: a) Raw TOA data. b) TOA data after mitigating Tx-Rx delay error. c) TOA data with outliers removed. d) Smoothed TOA data after passing through a clamped smoothing filter.

where x_i and y_i are the coordinates of base station i , x and y are the coordinates of the point to be solved, and r_i is the observation measurement from base station i .

Expanding equation (6), we get

$$x_i^2 + y_i^2 + x^2 + y^2 - 2x_i x - 2y_i y = r_i^2 \quad (8)$$

Let

$$K_i = x_i^2 + y_i^2 \quad (9)$$

$$R = x^2 + y^2 \quad (10)$$

Substituting equations (8) and (9) into (7), we obtain

$$r_i^2 - K_i = -2x_i x - 2y_i y + R \quad (11)$$

Then, N base stations can be represented as

$$\begin{bmatrix} r_1^2 - K_1 \\ r_2^2 - K_2 \\ \dots \\ r_N^2 - K_N \end{bmatrix} = \begin{bmatrix} -2x_1 & -2y_1 & 1 \\ -2x_2 & -2y_2 & 1 \\ \dots & \dots & \dots \\ -2x_N & -2y_N & 1 \end{bmatrix} \begin{bmatrix} x \\ y \\ R \end{bmatrix} \quad (12)$$

Simplifying, we get

$$Y = AX \quad (13)$$

Based on the least squares method, the coordinates can be solved.

$$\hat{p}_{llop} = X = (A^T A)^{-1} A^T Y \quad (14)$$

In the Kalman Filter part, the current position state value at time k is predicted based on the position state estimate at time $k-1$. This can be represented by [12]

$$\hat{x}_k^- = F \hat{x}_{k-1} + B \hat{p}_{llop_{k-1}} \quad (15)$$

$$P_k^- = F P_{k-1} F^T + Q \quad (16)$$

where \hat{x}_k^- is the prior estimate value at time k , \hat{x}_{k-1} is the posterior estimate value at time $k-1$, $\hat{p}_{llop_{k-1}}$ is considered as the input quantity of the llop part at time $k-1$ to the Kalman part, P_k^- is the prior covariance matrix at time k , P_{k-1} is the posterior covariance matrix at time $k-1$, and Q is the covariance matrix of the process noise.

After the prediction, the measurement update process is performed as follows:

$$K_k = P_k^- C^T (C P_k^- C^T + R)^{-1} \quad (17)$$

$$P_k = (I - K_k C) P_k^- \quad (18)$$

$$\hat{p}_{llop\&kf_k} = \hat{x}_k = \hat{x}_k^- + K_k (y_k - C \hat{x}_k^-) \quad (19)$$

where K_k represents the Kalman gain at time k , R is the measurement noise matrix, \hat{x}_k is the posterior estimate value at time k , y_k is the actual observation value, P_k is the posterior covariance matrix at time k . Based on these, the position coordinates estimated by the llop-KF algorithm can be obtained as $\hat{p}_{llop\&kf_k}$.

The Taylor algorithm is a recursive algorithm that requires knowledge of the initial estimate value of the target node. With each recursion, the algorithm improves the estimated coordinates of the target node by solving a local least squares solution for the TDOA measurement error. In the preceding text, the position coordinates estimated by the llop-KF algorithm, $\hat{p}_{llop\&kf_k}$, are

computed. Then, using this point as the initial point for the Taylor algorithm, the algorithm iteratively approaches the true point through multiple iterations.

When there is an error between the estimated coordinates and the true coordinates due to the algorithm [13]

$$\begin{aligned} TDOA_{i1} &= TOA_i - TOA_1 \\ &= \sqrt{(x_i - x)^2 + (y_i - y)^2} - \sqrt{(x_1 - x)^2 + (y_1 - y)^2} + n_{i1}, i = 2, 3 \dots N \end{aligned} \quad (20)$$

Assuming that point (x, y) represents the true coordinates of the target to be measured, the estimated coordinates (\hat{x}, \hat{y}) can be expressed as follows:

$$\begin{cases} \hat{x} = x + \delta_x \\ \hat{y} = y + \delta_y \end{cases} \quad (21)$$

The first-order Taylor expansion at point (\hat{x}, \hat{y}) is given by:

$$TDOA_{i1} - n_{i1} \approx \sqrt{(x_i - \hat{x})^2 + (y_i - \hat{y})^2} - \sqrt{(x_1 - \hat{x})^2 + (y_1 - \hat{y})^2} + a_{i1}\delta_x + a_{i2}\delta_y \quad (22)$$

where

$$\begin{cases} a_{i1} = \frac{\delta f_i(x,y)}{\delta x} |_{\hat{x}, \hat{y}} = \frac{(x_i - \hat{x})}{TOA_i} - \frac{(x_1 - \hat{x})}{TOA_1} \\ a_{i2} = \frac{\delta f_i(x,y)}{\delta y} |_{\hat{x}, \hat{y}} = \frac{(y_i - \hat{y})}{TOA_i} - \frac{(y_1 - \hat{y})}{TOA_1} \end{cases} \quad (23)$$

Simplifying the above equation, we get

$$Y = HX + e \approx HX \quad (24)$$

where

$$H = \begin{bmatrix} a_{21} & a_{22} \\ a_{31} & a_{32} \\ \dots & \dots \\ a_{n1} & a_{n2} \end{bmatrix}, X = \begin{bmatrix} \delta_x \\ \delta_y \end{bmatrix}, Y = \begin{bmatrix} TDOA_{21} - (TOA_2 - TOA_1) \\ TDOA_{31} - (TOA_3 - TOA_1) \\ \dots \\ TDOA_{n1} - (TOA_n - TOA_1) \end{bmatrix}, e = \begin{bmatrix} n_{21} \\ n_{31} \\ \dots \\ n_{n1} \end{bmatrix} \quad (25)$$

According to the Weighted Least Squares (WLS) method, we can obtain

$$X = (H^T Q^{-1} H)^{-1} H^T Q^{-1} Y \quad (26)$$

where Q represents the covariance matrix of the TDOA measurements. We set a threshold Φ , and when $\Phi < |\delta_x| + |\delta_y|$, we update the initial values (x_0, y_0) before the iteration as follows:

$$\begin{cases} x_{0_n} = x_{0_{n-1}} + \delta_x \\ y_{0_n} = y_{0_{n-1}} + \delta_y \end{cases} \quad (27)$$

Repeat the iteration until $|\delta_x| + |\delta_y|$ is less than the threshold value. Then, the initial values (x_0, y_0) from the previous iteration are obtained as follows:

$$\hat{p}_{B_k} = (x_{0_{n-1}}, y_{0_{n-1}}) \quad (28)$$

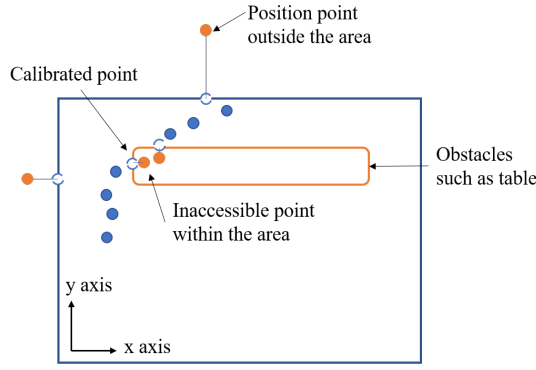


Figure 6: Position Correction Illustration.

2.3. Position Fusion

As time passes, the localization accuracy of Module A may gradually decrease, while the delay error of Tx-RX is taken from the mean value of multiple sets of data. Therefore, the localization accuracy of Module A decreases faster than that of Module B. In the localization fusion part, we set a value λ . When the absolute difference between \hat{p}_{B_k} and \hat{p}_{A_k} is less than λ , we perform weighted fusion based on the RMSE of the two localization estimates. When the absolute difference between \hat{p}_{B_k} and \hat{p}_{A_k} is greater than λ , we use \hat{p}_{B_k} only as the final solution. The above process can be expressed as follows:

$$\hat{p}_k = \begin{cases} \frac{RMSE_B}{RMSE_A + RMSE_B} \hat{p}_{A_k} + \frac{RMSE_A}{RMSE_A + RMSE_B} \hat{p}_{B_k}, & abs(\hat{p}_{B_k} - \hat{p}_{A_k}) < \lambda \\ \hat{p}_{B_k}, & abs(\hat{p}_{B_k} - \hat{p}_{A_k}) > \lambda \end{cases} \quad (29)$$

The position estimate after fusion, \hat{p} , can be obtained from the above equation.

2.4. Trajectory Correction

In the final step of the positioning trajectory correction, this part can be ignored if the relevant prior information about the target area is not available. However, if certain prior information is known, such as the length and width of the positioning area or the specific positions of partitions and tables within the area, the solution results can be corrected. The schematic diagram of the correction process is shown in **Figure 6**.

In the figure, the orange dots represent the coordinates to be corrected, while the hollow dots represent the coordinates after correction.

3. Experiments and Results

The experimental environment is a representative indoor office space located in Huawei Chengdu Building. The dimensions of the office are 15m in length and 15m in width, with a fixed ceiling

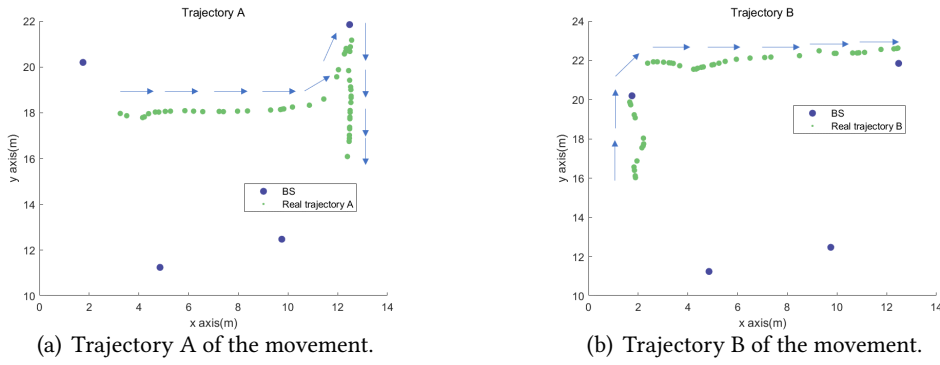


Figure 7: Ground truth trajectory of the movement.

Table 1

Module A Positioning Error

Motion trajectory	RMSE(m)	MAE(m)	75% error(m)
Trajectory A	1.0081	0.9166	1.1845
Trajectory B	0.8023	0.6975	0.8338

height of 3.2m. Within the room, there are various office furniture, such as desks, chairs, and partitions, with heights ranging from 0.5m to 1.5m. Four known base stations are installed at the corners of the ceiling [14].

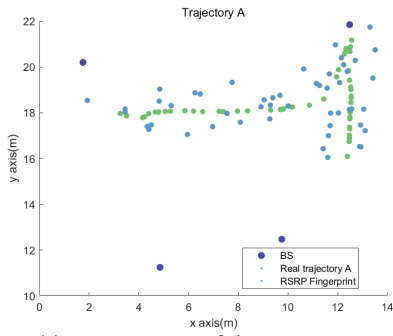
To validate the positioning algorithm's performance in different reachable areas within the environment, two trajectory patterns were chosen for the experiments, as illustrated in **Figure 7**.

In the experiment, the user equipment (UE) was a Huawei Mate 30 Pro terminal, fixed on a cart at a height of 1.2m and moved slowly at a speed of 0.2 – 0.5m/s. During the movement, the UE transmitted probing reference signals (SRS) to all TRPs in the room, and each TRP measured and recorded the time of arrival (TOA) and reference signal received power (RSRP) of the SRS signal. The transmission period of the SRS signal was 80ms, and two sets of experiments were conducted for approximately 85 seconds to obtain Trajectory A and Trajectory B, respectively (each set included 1000 measurements). Finally, to evaluate the positioning accuracy of the algorithm, this paper calculated the root mean square error (RMSE), mean absolute error (MAE), and 75% error based on 50 ground truth locations from the 1000 measurements as performance evaluation metrics.

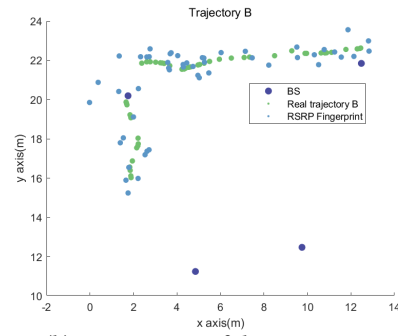
3.1. Estimated Results from the Neural Network Section of Module A

The estimated positioning trajectory for Module A is shown in **Figure 8**. The CDF plots for these two cases are shown in **Figure 9**. The RMSE, MAE, and 75th percentile error are shown in **Table 1**.

As can be seen from **Figure 8**, although some points fitted by the RNN based on the historical

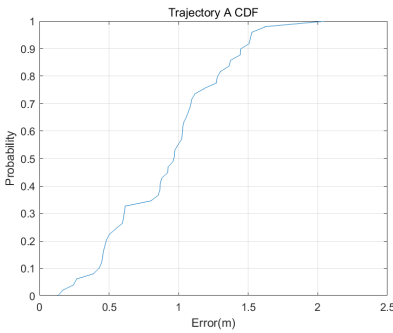


(a) Trajectory A of the movement.

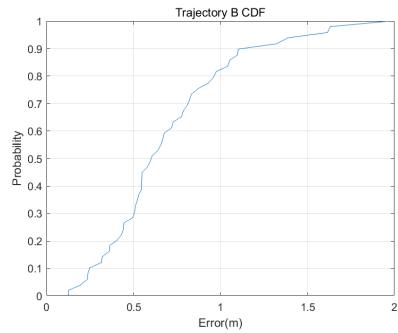


(b) Trajectory B of the movement.

Figure 8: The position estimation results of Module A compared with the ground truth trajectories.



(a) Trajectory A of the movement.



(b) Trajectory B of the movement.

Figure 9: The CDF plot of position error.

trajectory have a certain distance from the true points, they are generally distributed evenly around the rough outline of the true trajectory. The RNN can well fit the actual movement trajectory, and it has a good positioning result.

3.2. Module B Positioning Solution Results

The positioning trajectory A for Module B is depicted in **Figure 10**, while the trajectory B is shown in **Figure 11**. For better observation, some outliers in trajectory A were ignored and the CDF curves were plotted in both cases as shown in **Figure 12**. The RMSE, MAE, and 75th percentile errors are shown in **Table 2**.

From the trajectories shown in Figures 11 and 12, it can be observed that without TOA smoothing, using the Taylor algorithm to approximate the true points may result in certain points failing to converge in the recursive process of the Taylor algorithm due to significant fluctuations in the TOA data. As a result, large positioning errors may occur. However, after applying TOA smoothing prior to the Taylor approximation, as indicated by the purple dots in the figures, all the positioning points achieve a satisfactory approximation to the true points at their initial positions.

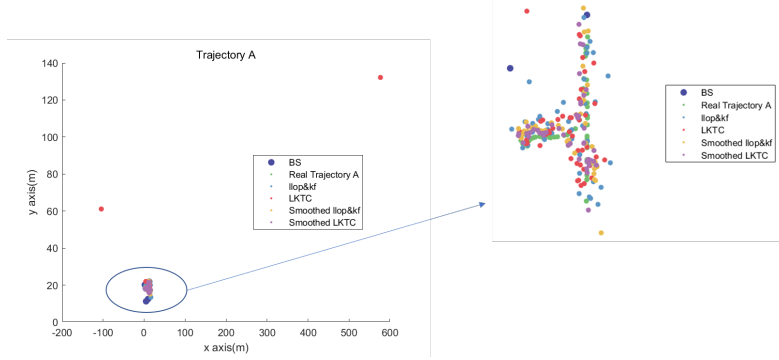


Figure 10: Positioning Results of Trajectory A using TOA Solution

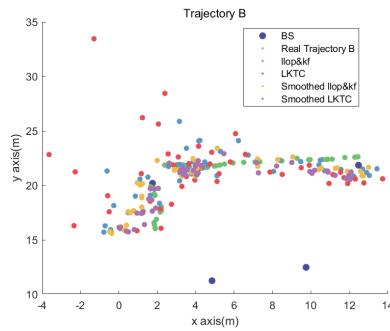


Figure 11: Positioning Results of Trajectory B using TOA Solution

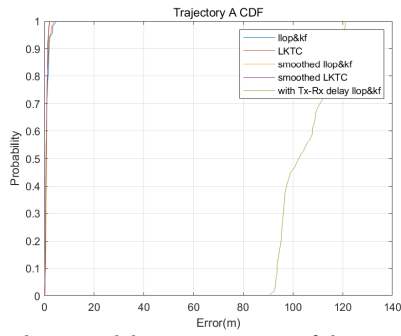
Table 2

Module B Positioning Error

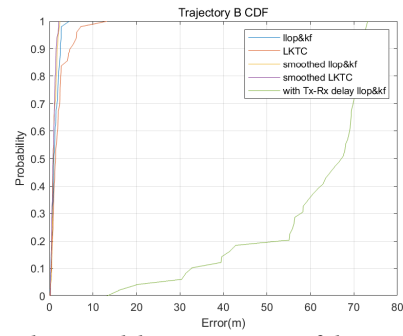
Motion trajectory	Method	RMSE(m)	MAE(m)	75% error(m)
Trajectory A	llop-KF	1.3171	0.9604	1.2260
	LKCT	83.2916	14.8606	1.1649
	Smoothed llop-KF	0.9977	0.9052	1.1443
	Smoothed LKCT	0.8562	0.7331	0.9889
Trajectory B	llop-KF	1.5783	1.3000	1.9210
	LKCT	3.1206	2.1236	2.4296
	Smoothed LKCT	1.0363	0.9092	1.1846

3.3. Fused Positioning Results

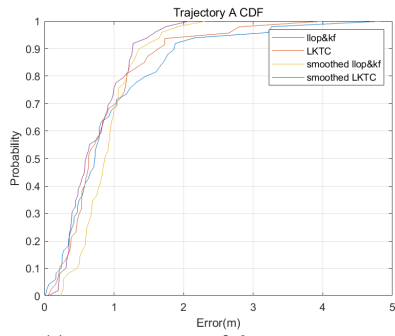
This part combines the smoothed LKCT positioning results with the RSRP fingerprint positioning results, and the fused positioning estimated trajectory is shown in **Figure 13**. The CDF plots for these two scenarios are shown in **Figure 14**. The RMSE, MAE, and 75th percentile errors are shown in **Table 3**.



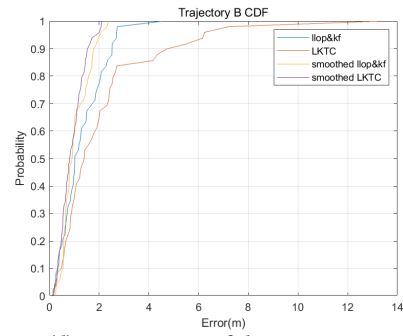
(a) With Tx-Rx delay Trajectory A of the movement.



(b) With Tx-Rx delay Trajectory B of the movement.

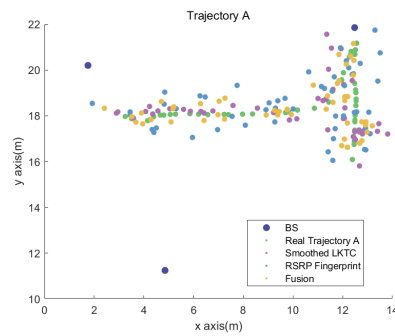


(c) Trajectory A of the movement.

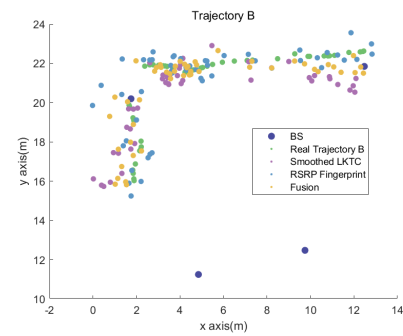


(d) Trajectory B of the movement.

Figure 12: The CDF plot of TOA position error.



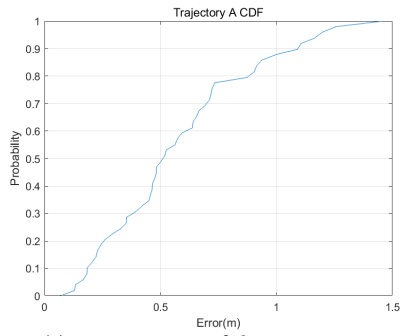
(a) Trajectory A of the movement.



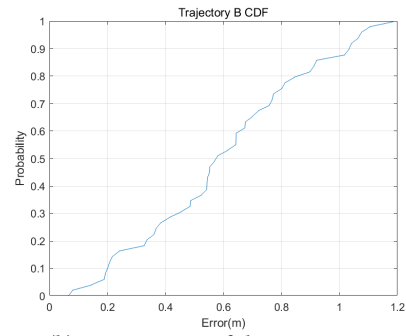
(b) Trajectory B of the movement.

Figure 13: Fused Estimated Trajectories with Ground Truth Trajectories.

From the trajectory in Figure 13, it can be observed that some of the points with relatively large deviations in the RSRP-based positioning result are evenly distributed on both sides of the true trajectory, while in the TOA-based positioning result, there are some points biased towards one side of the true trajectory. By fusing the two positioning results using a residual variance fusion strategy, the positioning system corrected to some extent the part of the TOA estimation that deviated significantly, pulling it towards the true trajectory and achieving a



(a) Trajectory A of the movement.



(b) Trajectory B of the movement.

Figure 14: Fused Position Error CDF Plot.

Table 3

Fused Positioning Error

Motion trajectory	RMSE(m)	MAE(m)	75% error(m)
Trajectory A	0.6623	0.5756	0.7223
Trajectory B	0.6752	0.5979	0.8013

better positioning result.

4. Conclusion

This paper proposes a 5G TOA positioning method assisted by RSRP information. The method utilizes RSRP training data to train a historical trajectory RNN network compensating for the transmission and reception errors that occur in the hardware components from the baseband to the antenna. Additionally, a clamping smoothing filter is designed to mitigate errors caused by clock jitter. Finally, through a fusion strategy, the final positioning results are computed. Experimental results show that the RSRP-Assisted 5G Measurement Time-Based Position Method achieves a root mean square error of 0.68m, a mean error of 0.60m, and a 75% error of 0.80m, demonstrating favorable positioning accuracy.

We will continue to explore the potential of integrating traditional positioning algorithms with artificial intelligence-based positioning methods, paving the way for future advancements in this field.

Acknowledgments

This work is financially supported by National Key R&D Program of China (No. 2022YFB2601801).

References

- [1] O. Kanhere and T. S. Rappaport, "Position Location for Futuristic Cellular Communications: 5G and Beyond," in *IEEE Communications Magazine*, vol. 59, no. 1, pp. 70-75, January 2021, doi: 10.1109/MCOM.001.2000150.
- [2] D. Dogan, Y. Dalveren and A. Kara, "A Mini-Review on Radio Frequency Fingerprinting Localization in Outdoor Environments: Recent Advances and Challenges," 2022 14th International Conference on Communications (COMM), Bucharest, Romania, 2022, pp. 1-5, doi: 10.1109/COMM54429.2022.9817189.
- [3] R. Keating, M. Säily, J. Hulkkonen and J. Karjalainen, "Overview of Positioning in 5G New Radio," 2019 16th International Symposium on Wireless Communication Systems (ISWCS), Oulu, Finland, 2019, pp. 320-324, doi: 10.1109/ISWCS.2019.8877160.
- [4] M. Atia, A. Noureldin, and M. Korenberg, "Dynamic online-calibrated radio maps for indoor positioning in wireless local area networks," *IEEE Trans. Mobile Comput.*, vol. 12, no. 9, pp. 1774– 1787, Sep. 2013.
- [5] Ren, Bin, et al. "Progress of 3GPP Rel-17 Standards on New Radio (NR) Positioning." IPIN-WiP. 2021.
- [6] Y. Ji, S. Biaz, S. Pandey, and P. Agrawal, "ARIADNE: A dynamic indoor signal map construction and localization system," in *Proc. 4th Int. Conf. Mobile Syst. Appl. Services*, 2006, pp. 151–164.
- [7] H. Wang, S. Sen, A. Elgohary, M. Farid, M. Youssef, and R. R. Choudhury, "No need to war-drive: Unsupervised indoor localization," in *Proc. 10th Int. Conf. Mobile Syst. Appl. Services*, 2012, pp. 197–210.
- [8] 3GPP, CATT, "Discussion on accuracy improvements by mitigating UE Rx/Tx and/or gNB Rx/Tx timing delays", R1-2104520, May 2021.
- [9] Gu, Shuang, Xiaoming Ren, and Dengpan Li. "Design of high precision transient waveform measurement algorithm based on oversampling and mean filtering." *IOP Conference Series: Earth and Environmental Science*. Vol. 692. No. 2. IOP Publishing, 2021.
- [10] Wang, Y., Sun, D.-Y., Qi, Z.-G. (2017). "Aging simulation method for EFI engine oxygen sensor based on first order inertial filter algorithm." *Jilin Daxue Xuebao (Gongxueban)/Journal of Jilin University (Engineering and Technology Edition)*, 47(4), 1040–1047.
- [11] M. T. Hoang, B. Yuen, X. Dong, T. Lu, R. Westendorp and K. Reddy, "Recurrent Neural Networks for Accurate RSSI Indoor Localization," in *IEEE Internet of Things Journal*, vol. 6, no. 6, pp. 10639-10651, Dec. 2019, doi: 10.1109/JIOT.2019.2940368.
- [12] Shin, Junhyeok, and Hoeryoung Jung. "UWB/GPS Sensor Fusion Using Kalman Filter for Outdoor Autonomous Robot." 2022 22nd International Conference on Control, Automation and Systems (ICCAS). IEEE, 2022.
- [13] Ren, Jin, Jingxing Chen, and Wenle Bai. "A new localization algorithm based on Taylor series expansion for NLOS environment." *Cybernetics and Information Technologies* 16.5 (2016): 127-136.
- [14] Yi Wang, Qinxin Liu, "Track 8: "5G Positioning (off-site)" Special features," The EvAAL Framework, https://eval.aaloa.org/files/2022/Track-8_TA-2022.pdf, Aug, 2022.